BEAM HALO FORMATION AND LOSS INDUCED BY IMAGE-CHARGE EFFECTS IN A SMALL-APERTURE ALTERNATING-GRADIENT FOCUSING SYSTEM*

J. Zhou, B. L. Qian and C. Chen, MIT Plasma Science and Fusion Center, Cambridge, MA 02139
E. Henestroza, S. Eylon and S. Yu, Lawrence Berkeley National Laboratory, Berkeley, CA 94720

Abstract

Effects of image charges on beam halo formation and beam loss in small-aperture alternating-gradient focusing systems are studied analytically, computationally, and experimentally. Nonlinear image-charge fields result in chaotic particle motion and the ejection of particles from the beam core into a halo. Detailed chaotic particle motion and structure of the particle phase space is studied, and the beam loss rate is computed for a long transport channel. Image-charge effects are also studied for a short transport channel, and compared with the Neutralized Transport Experiment (NTX) at LBNL.

INTRODUCTION

An important aspect in the design of periodically focused beams in such accelerators is to prevent the beams from developing halos because they may cause beam losses to the conducting walls of the accelerating structures. The problem of halo formation and beam losses is of a serious concern in the design of small-aperture focusing transport systems that are often required in order to keep accelerator costs manageable. Two key mechanisms for halo formation have been studied using analytical models [1-3] and self-consistent simulations with particle-in-cell (PIC) techniques [4-7]. Until the present analysis, however, most published analytical results [1-3] on beam halo formation have been based on free-space models in which wall effects on halo formation have been ignored.

In this paper, we report a new mechanism for chaotic particle motion and halo formation in intense charge-particle beams. In particular, use is made of a test-particle model to investigate the dynamics of root-mean-squared (rms) matched intense charged particle beams propagating through an alternating-gradient quadrupole magnetic field and a small aperture. While the present model allows for nonuniform beams with elliptic symmetry, the effects of image charges on halo formation are illustrated with a uniform (KV) beam distribution [8]. It is shown that the image-charge-induced fields are nonlinear, and that they induce chaotic particle motion and halo formation.

We consider an rms-matched continuous intense charged-particle beam propagating in the longitudinal direction through an alternating-gradient quadrupole magnetic field with axial periodicity length S in a perfectly conducting round pipe with radius R. The beam density is assumed to be $n = n\left(x^2/a^2 + y^2/b^2\right)$. An analytical expression for the scalar potential can be obtained for the assumed density profile,

$$\begin{aligned}\phi &= -\pi abq\int_0^\infty \frac{ds}{\sqrt{\left(a^2+s\right)\left(b^2+s\right)}}\int_0^T n(T)\,dT \\ &+ \pi abq\left[\int_0^\infty \frac{ds}{\sqrt{\left(a^2+s\right)\left(b^2+s\right)}}\int_0^{T_1} n(T_1)\,dT_1 - 2\ln\left(\frac{R}{r}\right)\int_0^\infty n(T_1)\,dT_1\right]\end{aligned} \quad (1)$$

where

$T = x^2/\left(a^2+s\right) + y^2/\left(b^2+s\right)$, $T_1 = x_1^2/\left(a^2+s\right) + y_1^2/\left(b^2+s\right)$, $r = \left(x^2+y^2\right)^{1/2}$, $x_1 = R^2 x/\left(x^2+y^2\right)$, and $y_1 = R^2 y/\left(x^2+y^2\right)$.

For the KV beam, the periodic beam envelope functions $a(s) = a(s+S)$ and $b(s) = b(s+S)$ can be calculated from envelope equations [9]. Furthermore, in the paraxial approximation, the transverse equations of motion for an individual test particle can be obtained [3] with the potential in Eq. (1).

It is important to specify initial conditions for the test-particle motion that are consistent with the assumed beam density, which is accomplished by the particular choice of an initial distribution function [3] at $s = s_0$, i.e., $f_b(x,y,x',y',s_0) = N_b\delta(W-1)/\pi^2\varepsilon_x\varepsilon_y$, where $x' = dx/ds$, and W is the variable defined by $W = x^2/a^2 + (ax'-xa')^2/\varepsilon_x^2 + y^2/b^2 + (by'-yb')^2/\varepsilon_y^2$. Here, a, a', b, and b' denote the "initial" values at $s = s_0$.

IMAGE-CHARGE EFFECTS IN A LONG TRANSPORT CHANNEL

Using the model established in the previous section, we can investigate the halo formation and beam chaotic motion induced by the image-charge effects. For a long quadrupole focusing channel with the step-function lattice, the envelope functions $a(s)$ and $b(s)$ are obtained numerically and are benchmarked against the published results for the free-space case in [3]. The system parameters are chosen to be $\eta = 0.5$, $KS/\varepsilon_x = 10.0$, $\varepsilon_x = \varepsilon_y = \varepsilon$, and vacuum phase advance $\sigma_v = 80.0°$, which correspond to those in the High-Current Experiment (HCX) at LBNL [10]. The mechanism of beam loss is best illustrated by the phase space structure for the test-particle motion in the (x,x') plane as shown in Fig. 1, where the Poincaré surface-of-section plots for the trajectories of test particles are demonstrated for two cases: (a) free-space ($\hat{R} \equiv R/\sqrt{\varepsilon S} = \infty$) and (b) $\hat{R} = 4.5$. Forty one and twenty nine test particles are loaded

* Supported by the U. S. Department of Energy, Grant No. DE-FG02-95ER40919 and No. DE-FG02-01ER54662.

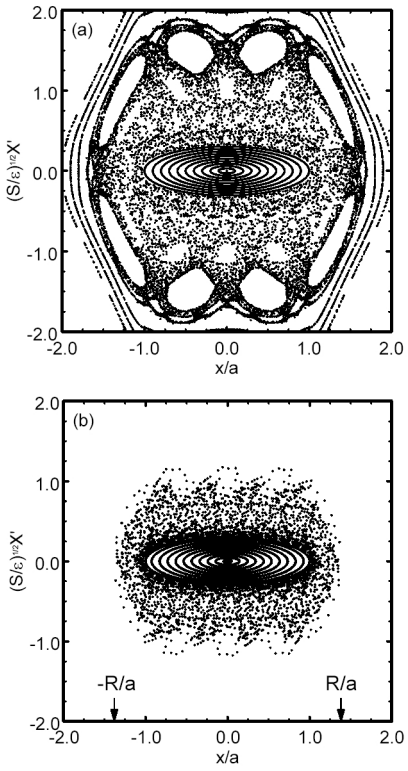

Fig.1 Poincaré surface-of section plots of test particles propagating over 1000 lattice periods in the phase plane (x, x') for two cases: (a) free-space $\hat{R} = \infty$ and (b) $\hat{R} = 4.5$.

uniformly at $s = 0$ between the intervals $-2.0 \le x' \le 2.0$ and $-1.32 \le x' \le 1.32$ along the x' - axis in Figs. 3(a) and 3(b), respectively. Because all of the test particles have $(y(0), y'(0)) = 0$, their trajectories remain in the (x, x') plane of the phase space. As shown in Fig.1 (a), well inside the beam with $W_x \le 1$ the motion is regular, whereas there is a chaotic sea bounded between $W_x = 1$ and an outer Kolmogorov-Arnold-Moser (KAM) surface at $x/a = 1.7$ for the free-space case with $\hat{R} = \infty$. This chaotic sea is fully connected; that is, a particle in the chaotic sea will fill out the entire region if it travels for a sufficiently long distance. As the pipe radius R decreases, the conductor wall intersects the chaotic sea as shown in Fig.1 (b), in which case the particles in the chaotic sea will eventually strike the wall.

It should be pointed out that as the pipe radius R decreases, the image effect on the dynamics of a beam with the KV distribution is subtle, as illustrated in Fig. 2. In Fig. 2 the transverse energy $W_x(s) = (x/a)^2 + (ax'/\varepsilon)^2$ is plotted as a function of the axial distance s for 50 test particles loaded at $s = 0$ on the beam boundary $W_x(0) = 1$ in the phase space with the initial phases $\phi_0 = \tan^{-1}\left[(S/\varepsilon)^{1/2} a(0)x'(0)/x(0)\right]$ uniformly distributed

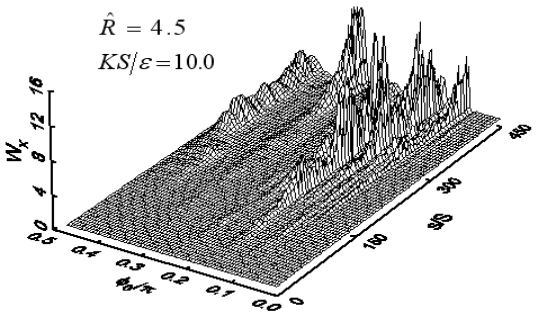

Fig. 2 Plots of W_x vs s for 50 test particles for $\hat{R} = 4.5$. The test particles are initially loaded uniformly with phase ϕ_0 ranging from 0 to $\pi/2$ on the beam boundary $(x(0)/a(0))^2 + (a(0)x'(0)/\varepsilon)^2 = 1$ in the phase space.

from 0 to $\pi/2$ for $\hat{R} = 4.5$. The system parameters are chosen to be the same as in Fig. 1. For the free-space case, the motion is stable, and the transverse energy is conserved with $W_x(s) = 1$ for all of the test particles. As R decreases to $\hat{R} = 4.5$, some test particles become chaotic due to the nonlinear force of the induced image charge on the wall, and the transverse energies of these particles are no longer constant.

Furthermore, the beam loss is computed as a function of propagation distance, and the results are shown in Fig. 3. The four curves correspond to four choices of the pipe radius with $\hat{R} = 3.8$, 3.9, 4.0, and 4.5. The beam loss rate increases with the decreasing pipe radius, where the image effects play a more important role in the total space charge force. When the maximum beam envelope fills 86% of the pipe, the beam loss reaches 8% at $s = 1000S$. Although the results shown in Fig. 3 are based on the test-particle calculations, they provide order of magnitude estimates for the actual beam losses, which are being studied using self-consistent simulations.

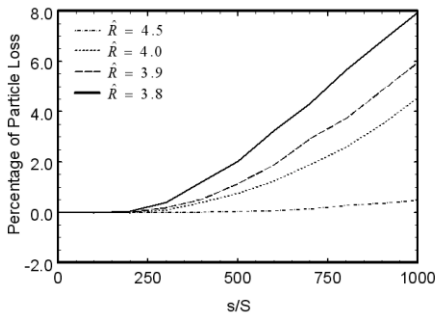

Fig. 3 Plots of the percentage of particles sticking the conductor wall as a function of propagation distance for several choices of $\hat{R} \equiv R/\sqrt{\varepsilon S}$. Here, 10,000 test particles with the KV distribution initially are used in the simulations.

Table 1. Simulation Parameters for NTX

Ion Energy:	300 KeV
Ion Current:	25 mA
Initial Beam Radius:	10 mm
Initial Beam Radius Derivative:	27 mr
Beam Velocity:	0.004 c
Magnetic Quadrupoles (T/m):	2.8,-3.62, 3.39, -1.95
Emittance ($4\pi \times rms$):	12π mm-mrad
Channel Length:	2.4 m
Final Circular Beam Radius:	20 mm
Final Beam Radius Derivative:	-20 mr
Pipe Radius:	75.8 mm

IMAGE-CHARGE EFFECTS IN NTX

We also use the theoretical model to analyze the NTX. Table 1 shows the simulation parameters for the NTX and Fig. 4 shows the beam envelopes. The focusing channel in the simulation is slight different from the experiment, and the emittance in the simulation is about 2 times the experimental value. Test-particles are put to propagating in the focusing channel of NTX to investigate image-charge effects for KV distribution beams.

Shown in Fig. 5 are the plots of the line-integrated phase plane distributions in (x,x') and (y,y') at the end of the channel, as obtained from the experimental measurements (left) and the simulation (right). The linear parts of x' and y' are subtracted in Fig. 5. There is no halo formation in the simulation for this short channel. However, the nonlinear forces induced by image charges create slight S-shaped and non-elliptic distributions in (x,x') and (y,y'), respectively, although we are still investigating the discrepancy between the experiment and theory regarding the orientation of the S-shaped distribution.

CONCLUSION

We have shown using a test-particle model that in a small-aperture alternating-gradient focusing channel, image-charge effects induce a new mechanism for chaotic particle motion and halo formation in intense charge-particle beams. The percentage of beam loss has been calculated as a function of propagating distance and aperture size. Because our results are obtained for ideal

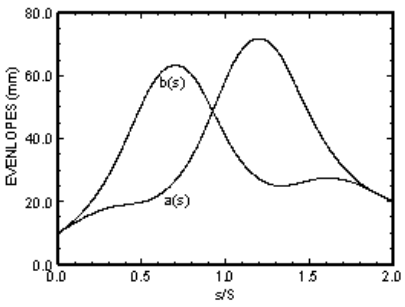

Fig. 4 Plots of the envelopes of the focusing channel of NTX.

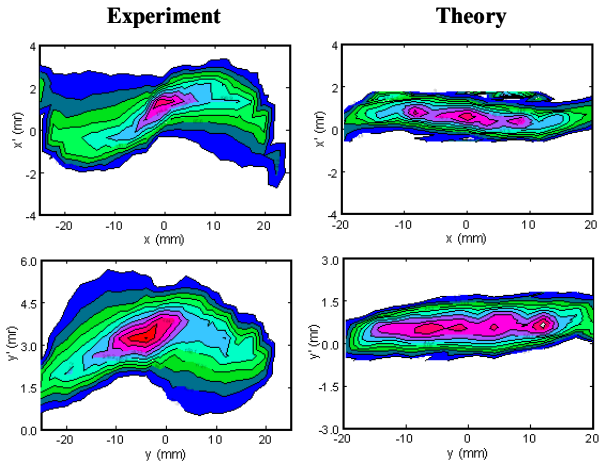

Fig. 5 Poincaré surface-of section plots of test particles at the end of NTX Channel in the phase plane (x,x') and (y,y').

KV distribution, they represent the minimum beam loss one may achieve in a long (>100 periods) focusing system such as the planned Integrated Research Experiment (IRE) for heavy ion fusion. They also suggest that in short (2 to 30 periods) systems such as the existing Neutralized Transport Experiment (NTX) and High-Current Experiment (HCX), imperfections such as charge-density fluctuations, mismatch, and focusing field nonlinearity and error may play more important role than image charge effects on beam halo production.

REFERENCES

1. R. L. Gluckstern, Phys. Rev. Lett. **73**, 1247 (1994).
2. J. M. Lagniel, Nucl. Instrum. Methods Phys. Res. **A345**, 405 (1994).
3. Q. Qian, R. C. Davidson, and C. Chen, Phys. Plasmas **2**, 2674 (1995); Phys. Rev. **E51**, R5216 (1995).
4. I. Haber, in *Proc. 1984 INS Int. Symposium on Heavy Ion Accelerators and Their Applications to Inertial Fusion* (Inst. Nuclear Study, Tokyo, 1984), p. 451.
5. C. M. Celata, in *Proc. 1987 Part. Accel. Conf.* (IEEE, New York, 1987), p. 996.
6. R. W. Garnett, *et al*., *Space Charge Dominated Beams and Applications of High Brightness Beams*, edited by S. Y. Lee, AIP Conf. Proc. No. **377** (AIP, New York, 1996), p. 60.
7. T. P. Waggler and J. Qiang, *Advanced Accelerator Concepts*, edited by C. E. Clayton and P. Muggli (AIP, Mandalay Beach, CA 2002), p. 878.
8. I. Kapchinskij and V. Vladimirskij, in *Proceedings of the International Conference on High Energy Accelerators and Instrumentation* (CERN Scientific Information Service, Geneva, 1959), p.274.
9. B. L. Qian, J. Zhou, and C. Chen, Phys. Rev. ST Accel. Beams **6**, 014201 (2003).
10. P. A. Seidl, F. M. Bieniosek, C. M. Celata *et al.,* Nucl. Instrum. Methods Phys. Res. **A464**, 369 (2001).